Special Collection

In Silico Characterization of Masitinib Interaction with SARS-CoV-2 Main Protease

Ulises Martínez-Ortega[+],[a] Diego I. Figueroa-Figueroa[+],[a] Francisco Hernández-Luis,[a] and Rodrigo Aguayo-Ortiz*[a]

Severe acute respiratory syndrome coronavirus 2 (SARS-CoV-2) infection continues to be a global health problem. Despite the current implementation of COVID-19 vaccination schedules, identifying effective antiviral drug treatments for this disease continues to be a priority. A recent study showed that masitinib (MST), a tyrosine kinase inhibitor, blocks the proteolytic activity of SARS-CoV-2 main protease (M^{pro}). Although MST is a potential candidate for COVID-19 treatment, a comprehensive analysis of its interaction with M^{pro} has not been done. In this work, we performed molecular dynamics simulations of the MST-M^{pro} complex crystal structure. The effect of the protonation states of M^{pro} H163 residue and MST titratable groups were studied. Furthermore, we identified the MST substituents and M^{pro} mutations that affect the stability of the complex. Our results provide valuable insights into the design of new MST analogs as potential treatments for COVID-19.

Coronavirus disease 2019 (COVID-19), caused by the severe acute respiratory syndrome coronavirus 2 (SARS-CoV-2), has caused an ongoing pandemic with more than 185 million cases and over 4.0 million deaths.[1] Currently, vaccines are being applied in numerous countries; however, more time is needed to reach levels that could control this global outbreak that would likely become a seasonal disease.[2,3] Despite some antiviral drugs received emergency authorization by different regulatory drug agencies around the world, their use are limited.[4] This situation elevates the need for specific antivirals that would help reduce morbidity and mortality caused by this disease.

To date, different druggable targets against SARS-CoV-2 have been identified for the development of a potential treatment, for example, RNA-dependent RNA polymerase (RdRp), papain-like protease (PL^{pro}), and main protease (M^{pro}).[5] The latter has gained relevance because, in addition to being vital for the viral life cycle, it has been observed that this enzyme prefers specific substrates not present in humans, speeding up the identification and design of molecules with high selectivity and low toxic effects.[6,7] Several peptidomimetics and small-molecules have been tested with good activity, which has led to the development of new M^{pro} covalent and non-covalent inhibitors.[8–11]

In this tireless effort to develop a molecule that could be a great solution to the problem caused by COVID-19, a recent study showed that masitinib (MST), a well-known tyrosine kinase inhibitor, had excellent inhibitory activity on M^{pro} (IC_{50} = 2.5 μM).[12] The MST-M^{pro} complex was solved by X-ray crystallography and deposited in the Protein Data Bank (PDB) (Figure 1A). Interestingly, MST was also identified as a M^{pro} inhibitor in a later high-throughput screening study carried out by another research group.[13] Despite MST could be a promising treatment for COVID-19, no further studies have been done to understand the interactions of MST with M^{pro} to design more active compounds.

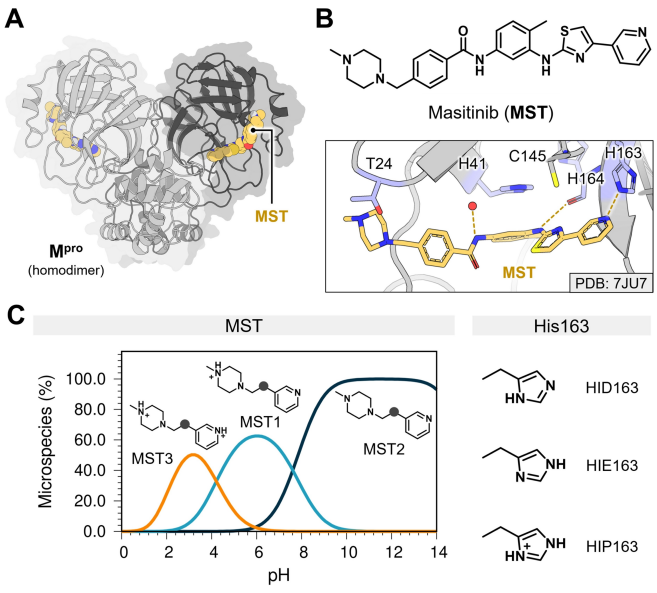

Figure 1. MST binding within M^{pro} homodimer active sites and protonation states. (A) Depiction of SARS-CoV-2 M^{pro} homodimer complexed with MST (PDB: 7JU7[12]). (B) MST binding mode and interaction with M^{pro} active site residues. MST is shown in stick format with its C atoms colored in yellow. Fundamental hydrogen bond interactions are shown as dashed lines. (C) Microspecies distribution of MST protonation states (MST1, MST2, and MST3) computed with Chemicalize[15] (left) and representation of the three H163 protonation states (HID163, HIE163, and HIP163) used in this study (right).

[a] U. Martínez-Ortega,[+] D. I. Figueroa-Figueroa,[+] Prof. F. Hernández-Luis, Prof. R. Aguayo-Ortiz
Departamento de Farmacia
Facultad de Química
Universidad Nacional Autónoma de México
Mexico City 04510 (Mexico)
E-mail: rodaguayo@comunidad.unam.mx

[+] These authors contributed equally to this work.

Supporting information for this article is available on the WWW under https://doi.org/10.1002/cmdc.202100375

Special Collection This article belongs to the Special Collection "BrazMedChem 2019: Medicinal Chemistry in Latin America".

Different computational approaches have been used to study the interaction of M^{pro} with other repositioned drugs, but none of them has studied MST.[14] In this work, we employed state-of-the-art computational approaches to study the dynamic behavior of this complex. We seek to understand the effect of MST and M^{pro} protonation states to provide critical information on such interactions that would lead us to identify MST regions that could be modified to enhance antiviral activity.

MST-M^{pro} complex crystal structure shows that MST binds non-covalently to both active sites on the M^{pro} homodimer (Figure 1A). Drayman et al.[12] identified three key interaction sites between MST and M^{pro} active site residues that block the recognition of virus-encoded polyproteins: (1) pyridine-H163 hydrogen bond, (2) thiazole-C145 hydrogen bond, and (3) toluene-H41 π-π stacking (Figure 1B). The last two listed interactions were pinpointed as the most relevant since they involve the two catalytic residues of the enzyme. However, upon closer inspection of the complex, it is possible to conclude that the hydrogen bond between the thiazole ring and the C145 side chain could not be taking place due to the weak interaction angle formed (94.7°). Although this intermolecular interaction seems unlikely, we detected during the structure checkup that a hydrogen bond could be formed between the amino group of the aminothiazole ring and the main chain carbonyl of H164. This intermolecular hydrogen bond has a suitable distance (3.0 Å) and angle (158.9°) to be considered a potential pharmacophoric point. In addition to the sites mentioned above, the high-resolution crystal structure of the MST-M^{pro} complex allowed the detection of the interaction of a water molecule with the carboxamide linker of MST. The stability of this structural water molecule at this site could result from being part of a bridge between the MST and the M^{pro}. On the other hand, the *N*-benzylpiperazine substituent of MST appears to have no interactions other than van der Waals. Throughout this work, we show the importance of all these interactions in the dynamic stability of the MST-M^{pro} complex and the factors that could modify MST binding to the M^{pro} active site (Table S1 of the SI).

It is well known that protonation of histidine residues at ε-nitrogen (HIE, neutral), δ-nitrogen (HID, neutral), or both (HIP, +1 charged) plays a crucial role in enzyme activity, protein stability, and protein-ligand interactions.[16] In a previous computational study, the importance of H163 side-chain interaction with covalent M^{pro} inhibitors was demonstrated.[17] The study also showed that H163 protonation at ε-nitrogen (HIE163 tautomer, Figure 1C) favors the formation of a hydrogen bond with several inhibitors that interact with the S1 specificity pocket. Therefore, to study the effect of the tautomerization and protonation of H163 on the interaction with the most abundant protomer of MST at pH 7 (MST1, Figure 1C), we carried out 200 ns molecular dynamics (MD) simulations of the homodimeric complex with the three different protonation states of H163 (Figure 2A and Figure S1 of the SI) using the Amber14SB[18] forcefield implemented in GROMACS 2019.6.[19] Root-mean-square deviation (RMSD) of MST1 relative to the M^{pro} backbone showed that MST1 has high mobility with HID163 and HIE163 states. On the other hand, a

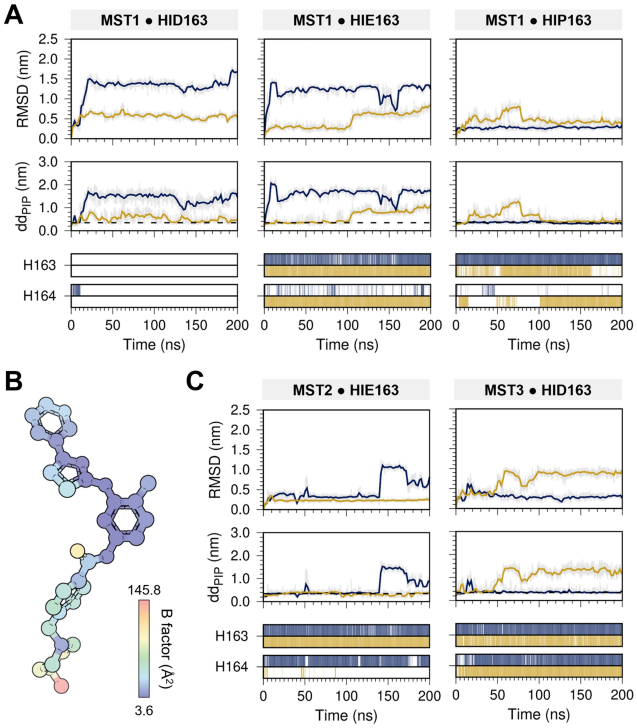

Figure 2. Effects of the protonation states of H163 residue and MST titratable groups in the MST-M^{pro} complex stability. RMSD of MST computed after least-square fit to M^{pro} backbone (top), minimum distance from the piperazine group to T24 and T45 residues (dd_{PIP}, middle), and hydrogen bonds of the pyridine ring with H163 and the aminothiazole with H164 (bottom) throughout the simulation time of the different protonation state systems of (A) H163 and (C) MST in the first (blue) and second (yellow) monomer of M^{pro}. The dotted black lines show the dd_{PIP} value of the crystal structure. (B) Depiction of MST structure color-coded by the B factor computed from the per-atom RMSF data.

lower fluctuation in the ligand positional RMSD was observed with the protonated form of H163 (HIP163). A recurring event during the simulations was the sudden RMSD changes of one of the ligands within the complex. By visual analysis of the MD simulations, we noticed that this variation in the RMSD was directly related to the high mobility of the *N*-benzylpiperazine moiety. The per-atom root-mean-square fluctuation (RMSF) of the MST1 heavy atoms confirmed this assertion (Figure 2B). In order to study this behavior, we measured the minimum distance (dd_{PIP}) between the piperazine group and two of the amino acids that constitute its binding pocket (T24 and T45). This parameter confirmed the direct relationship between the RMSD of the ligand position and the displacement of the *N*-benzylpiperazine group. In most cases, the result suggests that this group is displaced from its original position during the simulation and drastically modifies the MST binding mode. Therefore, we can conclude that the RMSD changes observed in the ligands were mainly due to the mobility of methylpiperazine.

Despite this conformational change, we could observe that, in some simulated systems, the rest of the MST structure remained in its initial position. To quantify this behavior, we analyzed the number of hydrogen bonds of (1) the pyridine

ring with the H163 imidazole side chain and (2) the aminothiazole ring with the H164 main chain carbonyl. The loss of all these hydrogen-bonding interactions demonstrated the low preference of MST1 for the M^{pro} homodimer containing the HID163 tautomer. On the other hand, conservation of the hydrogen bond between the pyridine ring and H163 residue in the HIE163 and HIP163 states suggests that this interaction is critical in stabilizing MST1 at the active site. Using the most stable MST1-M^{pro} complex of the homodimer, we found that MST1 formed hydrogen bonds with HIE163 and H164 during 51.0% and 81.6% of the MD simulation time. Conversely, the most stable complex containing HIP163 formed these hydrogen bond interactions only 78.9% (pyridine-HIP163) and 1.5% (aminothiazole-H164) of the time. Our result suggests that HIE163 is the most favorable protonation state for the stabilization and interaction of MST at the active site. In addition, this result agrees with that reported by Pavlova et al.,[17] in which the authors demonstrated, by using the Free Energy Perturbation (FEP) approach, that the transformation of HIE163 to HIP163 is unfavorable for the interaction of other M^{pro} inhibitors.

The next stage of our study focused on analyzing the influence of the unprotonated (MST2) and diprotonated (MST3) states of MST in the interaction with M^{pro} (Figure 2C). As with the previous systems, we performed 200 ns MD simulations of MST-M^{pro} complexes with the different protonation states. For MST3, in which the pyridine ring is in its protonated form, we decided to use the HID163 tautomer to promote the formation of the hydrogen bond interaction described above. We also carried out MD simulations of MST2-M^{pro} and MST3-M^{pro} with the HID163 and HIE163 tautomers, respectively, where the loss of interactions and dissociation of MST from the active site can be observed (Figure S2 of the SI). Figure 2C shows that both MST2 and MST3 have similar dynamic behavior observed in the MST1-M^{pro} complex with the HIE163 tautomer. Like the previous simulations, the *N*-benzylpiperazine moiety showed high mobility throughout the simulation time without affecting the hydrogen bonding interactions with histidines at positions 163 and 164. This result suggests that the stabilization of MST in the M^{pro} active site does not depend on its protonation state or mobility of the methylpiperazine group but the conservation of the hydrogen bonds with H163 and H164.

Based on our results, we performed two additional 200 ns MD simulations of the MST1-M^{pro} complex with the HIE163 tautomer as replicates to better analyze the implications of the methylpiperazine substituent binding mode and determine which interactions are critical to the complex stability (Figure S2 of the SI). Interestingly, the three independent MD simulations showed similar ligand RMSD distribution, *N*-benzylpiperazine group mobility, and hydrogen bonding interactions. It is worth mentioning that we evaluated the protein-ligand interactions of each monomeric complex of the last 170 ns for the three MD trajectories independently, giving a total of six MST1-M^{pro} systems. First, we carried out a clustering analysis based on the RMSD of MST1 after least-square fit to M^{pro} backbone. The clustering analysis allowed us to identify ten representative MST1 conformers, from which we determined the RMSD values distribution of each cluster population and the percentage of structures with an RMSD value lower than 0.25 nm (Figure 3A). From these, we observed that the most populated cluster (C01), with a mean RMSD value of 0.62 nm compared with MST1 binding mode in the crystal structure, had the *N*-benzylpiperazine portion out of the binding site. This result agrees with the analysis of our previous simulations, where we observed with the dd_{PIP} parameter that the piperazine was displaced from the initial position, leading to a substantial change in the RMSD value of MST1. Cluster 04 (C04), one of the most populated and with the lowest RMSD value (0.28 nm), presented an MST1 pose similar to that of the crystal structure. By comparing both MST1 structures, we were able to determine that the difference between both conformations was due to the rotation of the methylpiperazine group. It is noteworthy that C04 abundancy was less than 10% of the complete clustering analysis, which suggests that the high mobility of the *N*-benzylpiperazine moiety hinders the correct orientation of MST1 at the site during the simulation. Despite the displacement of this substituent, we found that in the 10 clusters (i.e., approximately 95% of all simulations), the rest of the structure (toluene-aminothiazole-pyridine) remained in its initial position and only exhibited slight conformational changes.

To further support this analysis, we calculated the fraction of contacts of MST1 (Q_{MST1}) with the M^{pro} residues located within a 4.0 Å radius around the ligand (Figure 3B). We found that residues near the *N*-benzylpiperazine in the crystal structure (i.e., T24, T25, C44, T45, S46, and E47) had fewer contacts with MST1 during the simulations. Interestingly, the rest of the MST1 structure formed many contacts ($Q_{MST1} \geq 0.8$) with the initial active site and S1 specificity pocket residues. This result confirms the high residence time of the MST1 at the binding site observed in the simulations. Based on the contact analysis and the critical interaction residues mentioned above, we characterized the occupancy fraction of the hydrogen bonds (HB), water bridges (WB), and π-π stacking (πS) interactions in the MST1-M^{pro} complexes (Figure 3C). This analysis showed that HB interactions of the methylpiperazine with the side chain of T24 and the main chain of S46 had an OF valor less than 0.03 due to the displacement of this group from the site. Also, the crystallographic water forming a WB between the amine group from the benzamide portion of MST1 and the H41 main chain carbonyl was considered. However, such interaction occurred very rarely during the simulations (OF = 0.07), suggesting that this WB interaction is dependent on the position of methylpiperazine and that the high mobility of this group hampers its formation.

On the other hand, πS interaction between the toluene ring and the imidazole of H41 and the HBs with H163 and H164 were formed for a longer time in the MD simulations (OF $>$ 0.32). Even though the OF value is relatively low, the MD analysis over time shows that these interactions are formed and broken throughout the trajectories and not only occur at the beginning of the simulation (Figure 2A and Figure S2 of the SI). These three interactions are essential to maintain MST1 within the binding site; such stability is also supported by our dihedral angle analysis (Figure 3D). This analysis showed that θ_1 dihedral

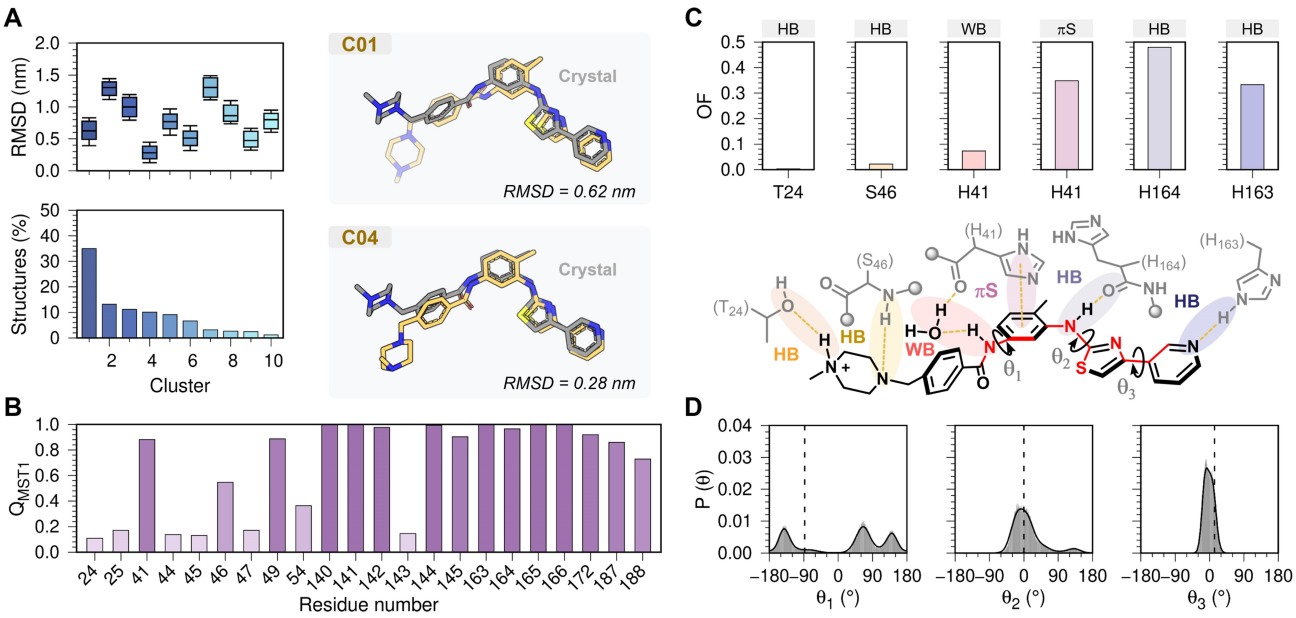

Figure 3. MD simulations analysis of the three independent replicas of MST1-M^{pro} homodimeric complex. (A) RMSD based clustering analysis of MST after least-square fit to M^{pro} backbone. RMSD distribution (top left) and percentage of structures in each cluster (bottom left). The box plot shows the full range of variation, from minimum to maximum, using the first (2.5%), second (50.0%), and third (97.5%) quantiles. Superposition of the most representative MST1 conformations from clusters C01 (yellow, top right) and C04 (yellow, bottom right) with the crystal structure (gray). (B) Fraction of the number of contacts of MST1 with M^{pro} residues (Q_{MST1}). (C) Occupancy fraction (OF) of hydrogen bond (HB), water bridge (WB), and π-π stacking (πS) interactions between MST1 and M^{pro} (top). Two-dimensional (2D) representation of MST1 within the binding site highlighting the six fundamental intermolecular interactions (bottom). (D) Dihedral angle distributions of the three rotatable bonds (θ_1 to θ_3) shown in the 2D interaction profile of section (C).

angle, formed by the bonds linking the benzamide group and toluenyl moiety, shows a rotation of this towards 65° and ±140°, which differ substantially from the angle in the crystal structure ($\theta_1 = -87.4$, dotted line in Figure 3D plots). This result also shows that the toluene ring, along with the rest of the MST1 structure, is not altered by the mobility of the *N*-benzylpiperazine group since only this angle is modified. On the other hand, θ_2 (bonds linking toluenyl moiety and 2-aminothiazole) and θ_3 (bonds linking pyridine moiety and 2-aminothiazole) dihedral angles did not exhibit significant changes when compared to the crystal structure. Moreover, the low variability registered in these dihedral angles facilitates the interaction of aminothiazole and pyridine rings of MST1 with M^{pro} binding site residues.

Our MD simulation results suggest that the *N*-benzylpiperazine portion of MST1 may not be essential for MST1-M^{pro} complex stability. Furthermore, none of the M^{pro} inhibitors reported to date occupy the methylpiperazine site, which means that this M^{pro} region does not play an essential role during inhibition.[20] Therefore, we made two modifications to the *N*-benzylpiperazine moiety of MST1 to support this hypothesis. The first modification led to the generation of a demethylated analog of MST1 (MSTA1, Figure 4A), which has already been co-crystallized with the SARS-CoV-2 M^{pro} (PDB: 7 L5D[21]). To confirm that the stability changes were mainly due to the methylpiperazine group, an analog without this was constructed from the MST coordinates on PDB: 7JU7 (MSTA2, Figure 4A) and leaving the benzamide ring unsubstituted. As in previous studies, we performed 200 ns MD simulations of the

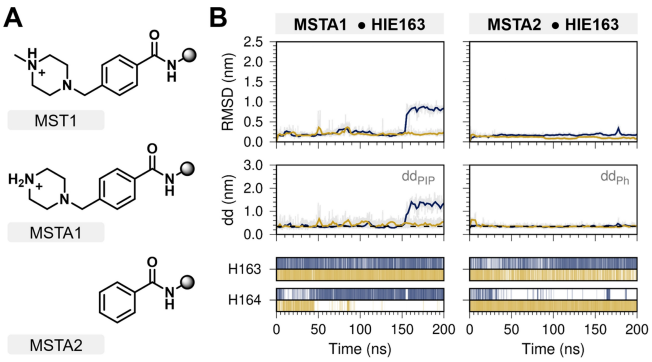

Figure 4. MD analysis of M^{pro} complexed with MST analogs. (A) Depiction of the partial chemical structures of MST1 and its analogs MSTA1 and MSTA2. (B) RMSD of MST analogs computed after least-square fit to M^{pro} backbone (top), minimum distance from the piperazine group (dd_{PIP}) or the phenyl ring (dd_{Ph}) to T24 and T45 residues (middle), and hydrogen bonds of the pyridine ring with H163 and the aminothiazole with H164 (bottom) throughout the simulation time in the first (blue) and second (yellow) monomer of M^{pro}.

M^{pro} homodimer complexed with each MST1 analogs. In these simulations, one of the MSTA1 molecules had a noticeable RMSD change near the end of the simulation time, which again was caused by the piperazine mobility. Interestingly, this RMSD "leap" was not observed in either of the two MSTA2-M^{pro} complexes, which confirms that the absence of the *N*-methylpiperazine group reduces the mobility of the ligand at the binding site and prevents its dissociation. Moreover, the minimum distance analysis between the phenyl group of the

benzamide and the T24 and T45 residues of M^{pro} (dd_{Ph}) confirmed that this substituent kept a similar position to that of the crystallographic structure during the simulation. Hydrogen bond analysis of MSTA2 with H163 and H164 in the more stable complex showed that these interactions were formed during 21.9% and 74.0% of the simulation time, similar to that observed in MST1-M^{pro} MD simulations. These results confirmed that the piperazine-like moiety is responsible for modifying the ligand stability and that the interactions of the rest of the MST structure with the active site have a similar profile despite the absence of this methylpiperazine group.

Finally, a total of 82 SARS-CoV-2 M^{pro} mutations were retrieved from the literature to identify those that could affect the binding of MST to M^{pro}.[22–24] Double free energy differences ($\Delta\Delta G_{bind} = \Delta G_{wildtype} - \Delta G_{mutant}$) of the 82 point mutations in the crystal MST1-M^{pro} complex and the distance between the mutated residues and MST1 ($dist_{Res\text{-}MST1}$) were computed using the mCSM-lig server[25] (Figure 5A and Table S2 of the SI). This server quantitatively predicts the effects of mutations on the stability of protein-ligand complexes with a standard error of 1.02 kcal/mol to 1.55 kcal/mol. In addition, the folding free energy difference ($\Delta\Delta G_{fold}$) calculated with the DUET algorithm[26] was used to determine the possible effect of these mutations on the M^{pro} structure. Of all the mutations studied, we found that only 5 of them are less than 10 Å away from MST1 ($dist_{Res\text{-}MST1} < 10$ Å), they do not significantly affect M^{pro} folding ($\Delta\Delta G_{fold} > -1.5$ kcal/mol) and have a destabilizing effect on the MST1-M^{pro} complex ($\Delta\Delta G_{bind} < -0.5$ kcal/mol). M49I ($\Delta\Delta G_{bind} = -1.2$ kcal/mol), D48E ($\Delta\Delta G_{bind} = -0.9$ kcal/mol), and P52S ($\Delta\Delta G_{bind} = -0.8$ kcal/mol) mutations affected the interaction of MST1 with M^{pro} to a greater extent since they are located very close to the active site of the enzyme, while K61R ($\Delta\Delta G_{bind} = -0.7$ kcal/mol) and N142S ($\Delta\Delta G_{bind} = -0.5$ kcal/mol) mutations had a lesser impact on the interaction as they were found in more distal sites. Noteworthy, the first three mutations could affect the interaction of any covalent or non-covalent inhibitors as they are close to the active site, hampering the optimization or design of new molecules. Conversely, the two last mutations play a less important role and have no direct implications on the binding of MST1 to M^{pro}. This result suggests MST1 structure optimization could be a good strategy for the design of new M^{pro} inhibitor agents.

In conclusion, our MD simulations demonstrate that three fundamental intermolecular interactions facilitate the stabilization of MST within the M^{pro} active site: (1) the hydrogen bond between the pyridine ring and the side chain of the HIE tautomer of H163, (2) the hydrogen bond formed between the amine of the aminothiazole ring with the main chain carbonyl of H164, and (3) the π-π stacking interaction of the toluenyl group with the imidazole ring of the catalytic H41 residue. Furthermore, we found that methylpiperazine, in any of the MST protonation states, affects the stability of the *N*-benzylpiperazine substituent. The removal of this group confirms the change in dynamic behavior and increase in the MST stability throughout the simulation time. Finally, we found that only 3 of the 82 mutations identified in M^{pro} could affect the stability of the MST1-M^{pro} complex. Although Touret et al.[27] found that imatinib-like kinase inhibitors do not prevent viral replication in hamster models, MST optimization based on the M^{pro} structure could avoid such problem. Our results provide essential information for the design of novel MST1 analogs with M^{pro} inhibitory activity that could be used as an alternative treatment against COVID-19.

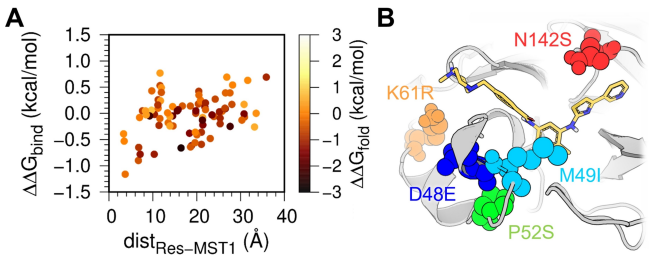

Figure 5. Effect of M^{pro} mutations on the binding of MST1. (A) Double free energy differences ($\Delta\Delta G_{bind}$) distribution of 82 M^{pro} point mutations against the distance between the mutated residues and MST1 ($dist_{Res\text{-}MST1}$) color-coded by the folding free energy difference ($\Delta\Delta G_{fold}$). (B) Depiction of the five most relevant destabilizing mutations of the MST1-M^{pro} complex identified within 10 Å of MST1.

Acknowledgments

U. M.-O. (1002367) and D.I. F.-F. (1002365) are very grateful to the Consejo Nacional de Ciencia y Tecnología (CONACyT) for the scholarships granted. R. A.-O. (LANCAD-UNAM-DGTIC-398) and F. H.-L. (LANCAD-UNAM-DGTIC-207) thank the Dirección General de Cómputo y de Tecnologías de Información y Comunicación (DGTIC) for the support received in the use of the HP Cluster Platform 3000SL supercomputer "Miztli".

Conflict of Interest

The authors declare no conflict of interest.

Keywords: SARS-CoV-2 · Main protease · Masitinib · Molecular dynamics · Protonation states

[1] World Health Organization, "Coronavirus (COVID-19) Dashboard," can be found under https://covid19.who.int/, **2021**.
[2] S. Bagcchi, *Lancet Infect. Dis.* **2021**, *21*, 323.
[3] S. Chen, K. Prettner, M. Kuhn, P. Geldsetzer, C. Wang, T. Bärnighausen, D. E. Bloom, *Sci. Rep.* **2021**, *11*, 9042.
[4] WHO Solidarity Trial Consortium,*N. Engl. J. Med.* **2021**, *384*, 497–511.
[5] I. Romeo, F. Mesiti, A. Lupia, S. Alcaro, *Molecules* **2021**, *26*, 632.
[6] J. Breidenbach, C. Lemke, T. Pillaiyar, L. Schäkel, G. Al Hamwi, M. Diett, R. Gedschold, N. Geiger, V. Lopez, S. Mirza, et al., *Angew. Chem. Int. Ed.* **2021**, *60*, 10423–10429.
[7] W. Rut, K. Groborz, L. Zhang, X. Sun, M. Zmudzinski, B. Pawlik, X. Wang, D. Jochmans, J. Neyts, W. Młynarski, et al., *Nat. Chem. Biol.* **2021**, *17*, 222–228.
[8] R. L. Hoffman, R. S. Kania, M. A. Brothers, J. F. Davies, R. A. Ferre, K. S. Gajiwala, M. He, R. J. Hogan, K. Kozminski, L. Y. Li, et al., *J. Med. Chem.* **2020**, *63*, 12725–12747.

[9] K. S. Yang, X. R. Ma, Y. Ma, Y. R. Alugubelli, D. A. Scott, E. C. Vatansever, A. K. Drelich, B. Sankaran, Z. Z. Geng, L. R. Blankenship, et al., *ChemMedChem* **2020**, 1–8.
[10] S. Günther, P. Y. A. Reinke, Y. Fernández-García, J. Lieske, T. J. Lane, H. M. Ginn, F. H. M. Koua, C. Ehrt, W. Ewert, D. Oberthuer, et al., *Science.* **2021**, *7945*, eabf7945.
[11] D. Suárez, N. Díaz, *J. Chem. Inf. Model.* **2020**, *60*, 5815–5831.
[12] N. Drayman, K. A. Jones, S.-A. Azizi, H. M. Froggatt, K. Tan, N. I. Maltseva, S. Chen, V. Nicolaescu, S. Dvorkin, K. Furlong, et al., *bioRxiv Prepr. Serv. Biol.* **2020**, 1–32.
[13] Y. Luo, F. Yu, M. Zhou, Y. Liu, B. Xia, X. Zhang, J. Liu, J. Zhang, Y. Du, R. Li, et al., *mBio* **2021**, *12*, 1–14.
[14] A. Gupta, H. X. Zhou, *ACS Comb. Sci.* **2020**, *22*, 826–832.
[15] M. Swain, *J. Chem. Inf. Model.* **2012**, *52*, 613–615.
[16] M. O. Kim, S. E. Nichols, Y. Wang, J. A. McCammon, *J. Comput.-Aided Mol. Des.* **2013**, *27*, 235–246.
[17] A. Pavlova, D. L. Lynch, I. Daidone, L. Zanetti-Polzi, M. D. Smith, C. Chipot, D. W. Kneller, A. Kovalevsky, L. Coates, A. A. Golosov, et al., *Chem. Sci.* **2021**, *12*, 1513–1527.
[18] J. A. Maier, C. Martinez, K. Kasavajhala, L. Wickstrom, K. E. Hauser, C. Simmerling, *J. Chem. Theory Comput.* **2015**, *11*, 3696–3713.
[19] M. J. Abraham, T. Murtola, R. Schulz, S. Páall, J. C. Smith, B. Hess, E. Lindah, *SoftwareX* **2015**, *1–2*, 19–25.
[20] H. M. Mengist, T. Dilnessa, T. Jin, *Front. Chem.* **2021**, *9*.
[21] K. Tan, N. I. Maltseva, R. P. Jedrzejczak, A. Joachimiak, *To be Publ.* **2021**.
[22] S. Vilar, D. G. Isom, *bioRxiv* **2020**, *2*, 1–18.
[23] T. J. Cross, G. R. Takahashi, E. M. Diessner, M. G. Crosby, V. Farahmand, S. Zhuang, C. T. Butts, R. W. Martin, *Biochemistry* **2020**, *59*, 3741–3756.
[24] O. S. Amamuddy, G. M. Verkhivker, Ö. T. Bishop, *J. Chem. Inf. Model.* **2020**, *60*, 5080–5102.
[25] D. E. V. Pires, T. L. Blundell, D. B. Ascher, *Sci. Rep.* **2016**, *6*, 1–8.
[26] D. E. V. Pires, D. B. Ascher, T. L. Blundell, *Nucleic Acids Res.* **2014**, *42*, W314–W319.
[27] F. Touret, J. S. Driouich, M. Cochin, P. R. Petit, M. Gilles, K. Barthélémy, G. Moureau, D. Malvy, C. Solas, X. de Lamballerie, et al., *bioRxiv* **2020**.

Manuscript received: May 27, 2021
Accepted manuscript online: June 17, 2021
Version of record online: July 9, 2021